

### Supporting Information

Fig. S1 (a) SEM image of TiO<sub>2</sub> nanorods arrays and (b) TEM block image

Fig. S2 XPS spectra of Ba<sub>0.8</sub>Sr<sub>0.2</sub>TiO<sub>3</sub>, Ba<sub>0.7</sub>Sr<sub>0.3</sub>TiO<sub>3</sub> and Ba<sub>0.3</sub>Sr<sub>0.7</sub>TiO<sub>3</sub>

Fig. S3 The applied bias photon-to-current efficiency (ABPE) of (a) Ba<sub>0.8</sub>Sr<sub>0.2</sub>TiO<sub>3</sub> and (b) Ba<sub>0.3</sub>Sr<sub>0.7</sub>TiO<sub>3</sub> photoanode

Fig. S4 UV-Vis absorption spectra of different doping concentrations corresponding to tauc plots of (a) Ba<sub>0.8</sub>Sr<sub>0.2</sub>TiO<sub>3</sub>; (b) Ba<sub>0.7</sub>Sr<sub>0.3</sub>TiO<sub>3</sub>; (c) Ba<sub>0.3</sub>Sr<sub>0.7</sub>TiO<sub>3</sub>

Fig. S5 The bulk charge separation efficiency of three different doping concentrations photoanodes

Fig. S6 Mott-Schottky plots of (a) Ba<sub>0.8</sub>Sr<sub>0.2</sub>TiO<sub>3</sub> and (b) Ba<sub>0.3</sub>Sr<sub>0.7</sub>TiO<sub>3</sub> photoanode

Tab. S1 Flat band potential ( $V_{fb}$ ) and donor density ( $N_A$ ) of Ba<sub>0.8</sub>Sr<sub>0.2</sub>TiO<sub>3</sub> electrodes deduced from Mott-Schottky

Tab. S2 Flat band potential ( $V_{fb}$ ) and donor density ( $N_A$ ) of Ba<sub>0.7</sub>Sr<sub>0.3</sub>TiO<sub>3</sub> electrodes deduced from Mott-Schottky

Tab. S3 Flat band potential ( $V_{fb}$ ) and donor density ( $N_A$ ) of Ba<sub>0.3</sub>Sr<sub>0.7</sub>TiO<sub>3</sub> electrodes deduced from Mott-Schottky

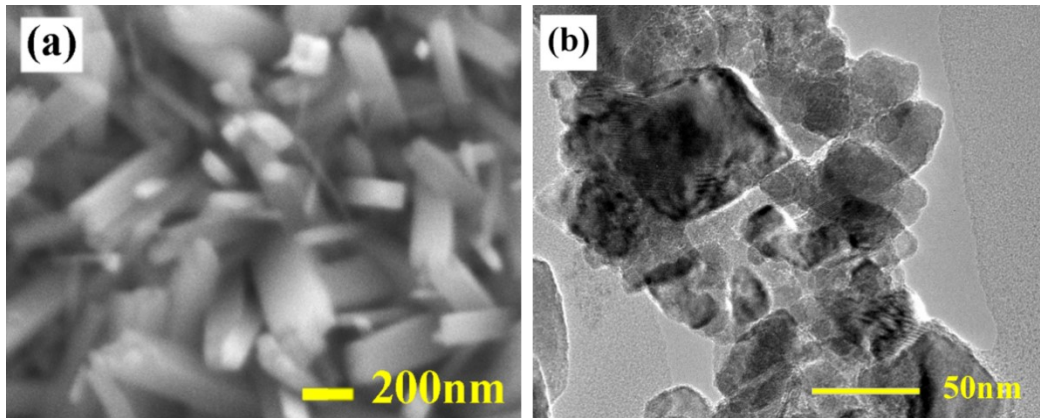


Fig. S1 (a) SEM image of TiO<sub>2</sub> nanorods arrays and (b) TEM block image

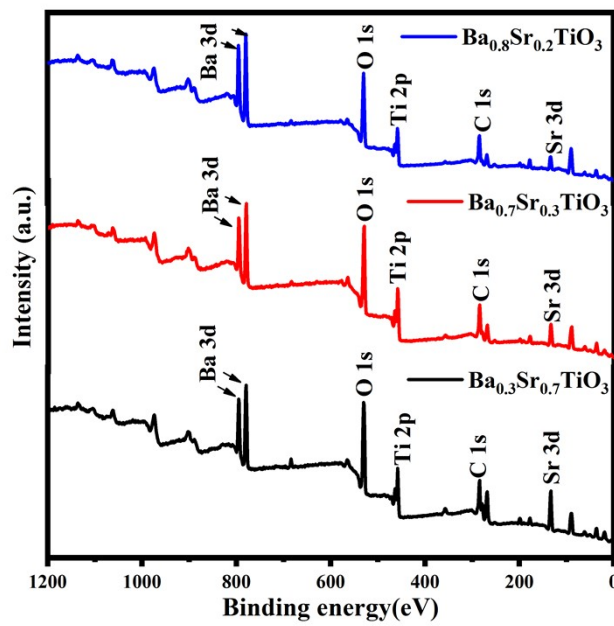


Fig. S2 XPS spectra of Ba<sub>0.8</sub>Sr<sub>0.2</sub>TiO<sub>3</sub>, Ba<sub>0.7</sub>Sr<sub>0.3</sub>TiO<sub>3</sub> and Ba<sub>0.3</sub>Sr<sub>0.7</sub>TiO<sub>3</sub>

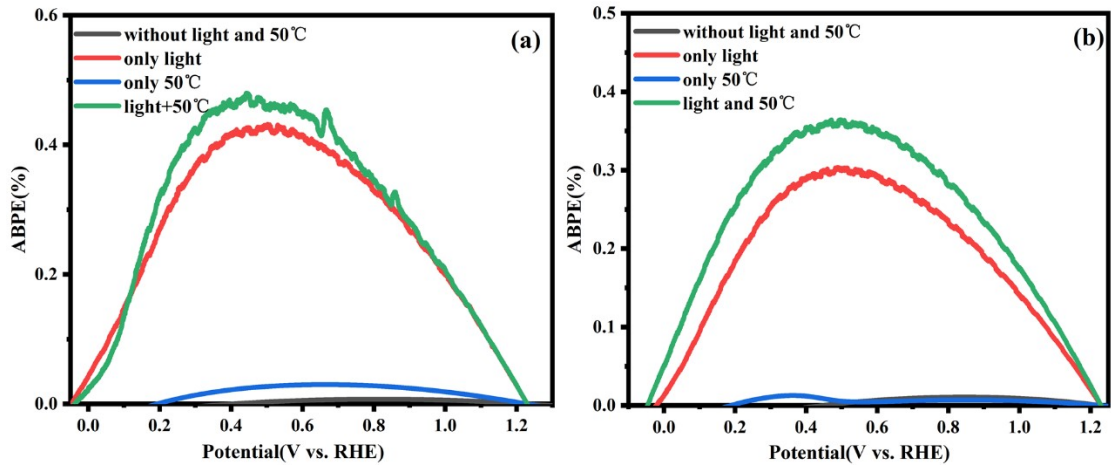


Fig. S3 The applied bias photon-to-current efficiency (ABPE) of (a)  $\text{Ba}_{0.8}\text{Sr}_{0.2}\text{TiO}_3$  and (b)  $\text{Ba}_{0.3}\text{Sr}_{0.7}\text{TiO}_3$  photoanode

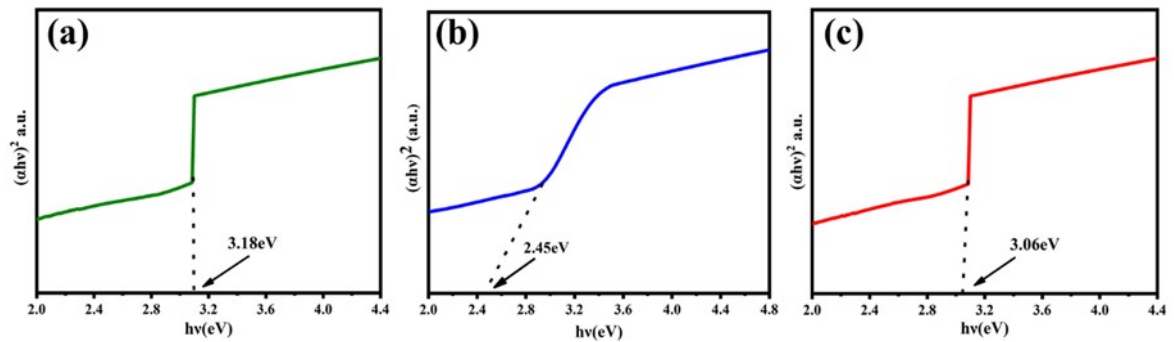


Fig. S4 UV-Vis absorption spectra of different doping concentrations corresponding to tauc plots of (a)  $\text{Ba}_{0.8}\text{Sr}_{0.2}\text{TiO}_3$ ; (b)  $\text{Ba}_{0.7}\text{Sr}_{0.3}\text{TiO}_3$ ; (c)  $\text{Ba}_{0.3}\text{Sr}_{0.7}\text{TiO}_3$

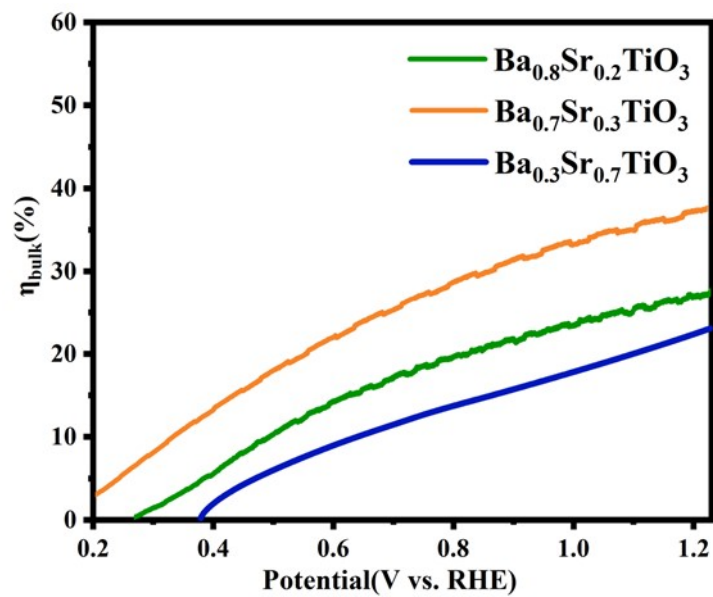


Fig. S5 The bulk charge separation efficiency of three different doping concentrations photoanodes

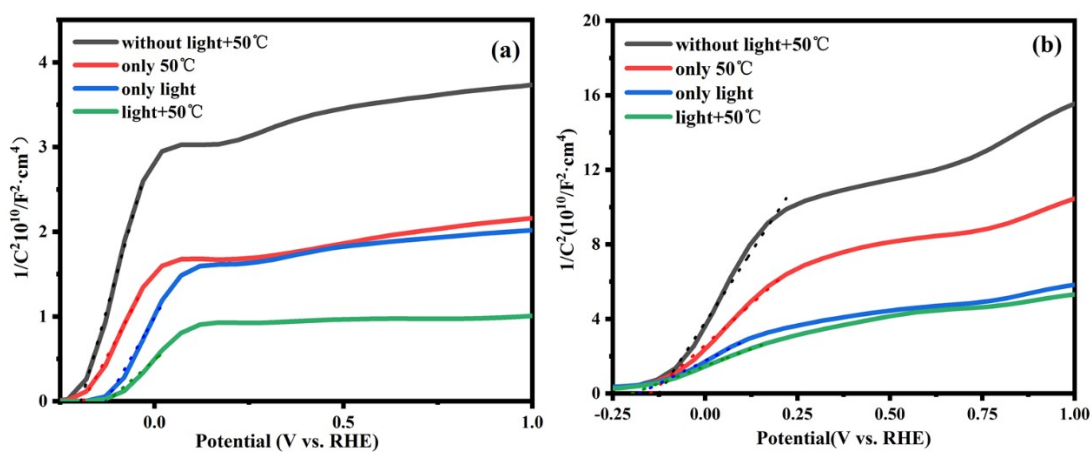


Fig. S6 Mott-Schottky plots of (a)  $\text{Ba}_{0.8}\text{Sr}_{0.2}\text{TiO}_3$  and (b)  $\text{Ba}_{0.3}\text{Sr}_{0.7}\text{TiO}_3$  photoanode

Tab. S1 Flat band potential ( $V_{fb}$ ) and donor density ( $N_A$ ) of  $Ba_{0.8}Sr_{0.2}TiO_3$  electrodes deduced from Mott-Schottky

Conditions	$V_{fb}$ (V vs. RHE)	$N_A$ ( $\times 10^{20} \text{ cm}^{-3}$ )
Dark	3.094	0.11
Only light	1.577	0.229
Only 50°C	0.989	0.211
Light and 50°C	0.487	0.452

Tab. S2 Flat band potential ( $V_{fb}$ ) and donor density ( $N_A$ ) of  $Ba_{0.7}Sr_{0.3}TiO_3$  electrodes deduced from Mott-Schottky

Conditions	$V_{fb}$ (V vs. RHE)	$N_A$ ( $\times 10^{20} \text{ cm}^{-3}$ )
Dark	0.834	0.18
Only light	0.245	3.46
Only 50°C	0.587	0.509
Light and 50°C	0.102	7.62

Tab. S3 Flat band potential ( $V_{fb}$ ) and donor density ( $N_A$ ) of  $Ba_{0.3}Sr_{0.7}TiO_3$  electrodes deduced from Mott-Schottky

Conditions	$V_{fb}$ (V vs. RHE)	$N_A$ ( $\times 10^{20} \text{ cm}^{-3}$ )
Dark	3.808	0.058
Only light	2.610	0.179
Only 50°C	1.759	0.100
Light and 50°C	1.473	0.237

